

Dexterity Analysis of the Tricept Manipulator

G. Pond¹, J. Carretero²

¹ *University of New Brunswick, Dept. of Mechanical Engineering, Geoff.Pond@UNB.ca,*

² *University of New Brunswick, Dept. of Mechanical Engineering, Juan.Carretero@UNB.ca*

The kinematics and workspace characteristics of the Tricept mechanism are studied. The inverse displacement solution is provided for the case where the independent degrees of freedom are defined as one translation and two rotations. An alternative solution to the inverse displacement problem is provided based on the elevation of three points on the end effector platform. This is then used in the formulation of a square dimensionally homogeneous Jacobian matrix whose condition number and singular values are then used to define the dexterous workspace. The influence of architectural parameters on both the reachable and dexterous workspace size is studied.

1 INTRODUCTION

Parallel manipulators have recently experienced more widespread attention as their various advantages become better known. They have been successfully implemented in applications where advantages such as high stiffness, potentially higher end effector velocities, and an ability to handle higher payloads, are of great importance. These characteristics are all of great importance when dealing with the application of manufacturing, or more specifically, machining.

One of the most notable parallel mechanisms to have been successfully implemented in the manufacturing industry is the Tricept manipulator [1]. Sparked by the success of this mechanism, and its curious architecture which includes 3 active and 1 passive limb (to be explained later), a variety of researchers have also taken interest, and made contributions in the development of this mechanism. Siciliano [2] developed the kinematics and studied the manipulability of the Tricept. Architectural optimization of the Tricept and similar mechanisms was undertaken by Zhang and Gosselin [3]. Most recently, the kinematics of this class of manipulator, having a passive leg, was discussed by Joshi and Tsai [4], and compared to that of a more conventional 3-UPU architecture, not having a passive leg [5]. Xi *et al* compared the reachable workspace characteristics of the Tricept to those of three other 3-DOF architectures [6]. This paper will further the previous works by determining the dexterous workspace size and furthermore, optimizing the architectural parameters to obtain the largest possible dexterous workspace size.

1.1 Dexterity

Most of the work introduced has studied the Tricept manipulator as a translational device, *i.e.*, having independent degrees of freedom (DOF) corresponding to translations in the x ,

y , and z axes. In this case, the Jacobian matrix \mathbf{J} which relates the actuator velocities $\dot{\mathbf{q}}$ and independent end effector velocities $\dot{\mathbf{x}}$ according to:

$$\dot{\mathbf{q}} = \mathbf{J}\dot{\mathbf{x}} \quad (1)$$

may be reduced to a 3×3 and is dimensionally consistent, as in [6]. This allows the use of conventional dexterity measures such as the condition number of the Jacobian matrix. However, now consider the case where instead of the three translations being desired, only a single translation and two rotations are desired, such as in [3]. Regardless of what conventional methods are used to formulate the Jacobian matrix, either by partial derivatives, screw theory, *etc.*, all lead to a dimensionally inconsistent Jacobian matrix.

Gosselin [7] introduced a method for planar mechanisms where the conventional end effector velocities (two translational velocities and one rotational velocity, all producing motion on the same plane) were modeled using the x , y components of the linear velocities of two points on the end effector. The ensuing Jacobian matrix mapping the three actuator velocities to the four linear velocities in the principle Cartesian directions, is dimensionally homogeneous. Kim and Ryu [8] have expanded this method to 6-DOF mechanisms using the x , y , and z components of the linear velocities of three points on the end effector. Pond and Carretero [9] have recently shown that these Jacobians relating the actuator velocities to end effector velocity vectors, $\dot{\mathbf{x}}$, containing both independent and dependent motions, as in [7] and [8] are unable to reliably measure the dexterity of the device as the physical significance of the Jacobian's singular values is unknown. Instead, the following method of formulating the Jacobian matrix was proposed in [9].

First consider Kim and Ryu's model of the Jacobian matrix for a Tricept manipulator having three prismatic actuators, and points A_i ($i = 1, 2, 3$) are three designated points fixed to the end effector. The variables in equation (1) are then:

$$\dot{\mathbf{q}} = [\dot{l}_1 \quad \dot{l}_2 \quad \dot{l}_3]^T \quad (2)$$

$$\mathbf{J} = \begin{bmatrix} \frac{\partial A_{1x}}{\partial l_1} & \frac{\partial A_{1y}}{\partial l_1} & \frac{\partial A_{1z}}{\partial l_1} & \frac{\partial A_{2x}}{\partial l_1} & \frac{\partial A_{2y}}{\partial l_1} & \frac{\partial A_{2z}}{\partial l_1} & \frac{\partial A_{3x}}{\partial l_1} & \frac{\partial A_{3y}}{\partial l_1} & \frac{\partial A_{3z}}{\partial l_1} \\ \frac{\partial A_{1x}}{\partial l_2} & \frac{\partial A_{1y}}{\partial l_2} & \frac{\partial A_{1z}}{\partial l_2} & \frac{\partial A_{2x}}{\partial l_2} & \frac{\partial A_{2y}}{\partial l_2} & \frac{\partial A_{2z}}{\partial l_2} & \frac{\partial A_{3x}}{\partial l_2} & \frac{\partial A_{3y}}{\partial l_2} & \frac{\partial A_{3z}}{\partial l_2} \\ \frac{\partial A_{1x}}{\partial l_3} & \frac{\partial A_{1y}}{\partial l_3} & \frac{\partial A_{1z}}{\partial l_3} & \frac{\partial A_{2x}}{\partial l_3} & \frac{\partial A_{2y}}{\partial l_3} & \frac{\partial A_{2z}}{\partial l_3} & \frac{\partial A_{3x}}{\partial l_3} & \frac{\partial A_{3y}}{\partial l_3} & \frac{\partial A_{3z}}{\partial l_3} \end{bmatrix} \quad (3)$$

$$\dot{\mathbf{x}} = [\dot{A}_{1x} \quad \dot{A}_{1y} \quad \dot{A}_{1z} \quad \dot{A}_{2x} \quad \dot{A}_{2y} \quad \dot{A}_{2z} \quad \dot{A}_{3x} \quad \dot{A}_{3y} \quad \dot{A}_{3z}]^T \quad (4)$$

Pond and Carretero [9] have introduced a constraining matrix to equation (1):

$$\dot{\mathbf{q}} = \mathbf{JP}\dot{\mathbf{x}}' \quad (5)$$

where the constraining matrix \mathbf{P} maps independent to dependent Cartesian velocities (where independent velocities may be defined for the Tricept as \dot{A}_{1z} , \dot{A}_{2z} , and \dot{A}_{3z}):

$$\mathbf{P} = \begin{bmatrix} \frac{\partial A_{1x}}{\partial A_{1z}} & \frac{\partial A_{1y}}{\partial A_{1z}} & 1 & \frac{\partial A_{2x}}{\partial A_{1z}} & \frac{\partial A_{2y}}{\partial A_{1z}} & 0 & \frac{\partial A_{3x}}{\partial A_{1z}} & \frac{\partial A_{3y}}{\partial A_{1z}} & 0 \\ \frac{\partial A_{1x}}{\partial A_{2z}} & \frac{\partial A_{1y}}{\partial A_{2z}} & 0 & \frac{\partial A_{2x}}{\partial A_{2z}} & \frac{\partial A_{2y}}{\partial A_{2z}} & 1 & \frac{\partial A_{3x}}{\partial A_{2z}} & \frac{\partial A_{3y}}{\partial A_{2z}} & 0 \\ \frac{\partial A_{1x}}{\partial A_{3z}} & \frac{\partial A_{1y}}{\partial A_{3z}} & 0 & \frac{\partial A_{2x}}{\partial A_{3z}} & \frac{\partial A_{2y}}{\partial A_{3z}} & 0 & \frac{\partial A_{3x}}{\partial A_{3z}} & \frac{\partial A_{3y}}{\partial A_{3z}} & 1 \end{bmatrix}^T \quad (6)$$

and

$$\dot{\mathbf{x}}' = [\dot{A}_{1z} \quad \dot{A}_{2z} \quad \dot{A}_{3z}]^T \quad (7)$$

The resulting multiplication of \mathbf{JP} is a 3×3 matrix mapping actuator velocities (\dot{l}_i) directly to independent end effector velocities (\dot{A}_{i_z}):

$$\mathbf{JP} = \begin{bmatrix} \frac{\partial l_1}{\partial A_{1z}} & \frac{\partial l_1}{\partial A_{2z}} & \frac{\partial l_1}{\partial A_{3z}} \\ \frac{\partial l_2}{\partial A_{1z}} & \frac{\partial l_2}{\partial A_{2z}} & \frac{\partial l_2}{\partial A_{3z}} \\ \frac{\partial l_3}{\partial A_{1z}} & \frac{\partial l_3}{\partial A_{2z}} & \frac{\partial l_3}{\partial A_{3z}} \end{bmatrix} \quad (8)$$

The singular values of this matrix have an evident meaning and may therefore be used in dexterity analysis. Before developing this Jacobian matrix for the Tricept manipulator, the inverse kinematics must first be solved.

2 KINEMATICS

The basic architecture of the Tricept mechanism is depicted in Figure 1a. Three identical, actuated limbs are connected to the exterior of the base and moving platform radii. These limbs consist of a spherical - prismatic - spherical (SPS) kinematic chain, where the prismatic joint is actuated. Alternatively, one of the spherical joints could be substituted with a universal joint with no consequence to the kinematic equations to be presented. In either case, as each of the actuated limbs has mobility of at least 6-DOF, a passive prismatic - universal (PU) limb exists at the centre of the mechanism to constrain the mobility of the moving platform to 3-DOF. In many works, the order of joints of the passive chain is interchanged to a UP limb (as opposed to the PU limb used in this paper). The resulting architectures are kinematically equivalent. However, regardless of the arrangement of the passive limb, in order to perform either of the two independent rotations, translation along either the x and y axes or a rotation around the z -axis may result. As in [10] these undesired, extraneous motions are termed parasitic motions. Intuitively, the magnitude of these parasitic motions is zero if the axes of the universal joint of the passive limb intersect at a point on the plane defined by the centres of the three spherical joints connecting the end effector platform to the actuated limbs. As the PU arrangement of the passive limb reduces or may even eliminate the defined parasitic motions, it is more beneficial in this application.

2.1 Inverse Kinematics

The independent degrees of freedom for the Tricept have been defined here as a translation along the z -axis (P_z), and rotations around the x and y axes of the fixed frame $\{O\}$, or angles ψ and θ respectively (see Figure 1a). The remaining parasitic motions are translations along the x and y axes (P_x and P_y respectively), and a rotation around the z -axis, ϕ . The rotation around the z -axis is of little interest considering that a machine tool, mounted on the end effector, is likely to have its spindle aligned with this axis anyhow. For that reason, the rotation matrix corresponding to this rotation is multiplied last in the following formulation of the overall rotation matrix relating the orientation of the moving frame $\{P\}$ to that of the base frame $\{O\}$:

$${}^O\mathbf{R}_P = \mathbf{R}_y(\theta) \mathbf{R}_x(\psi) \mathbf{R}_z(\phi) \quad (9)$$

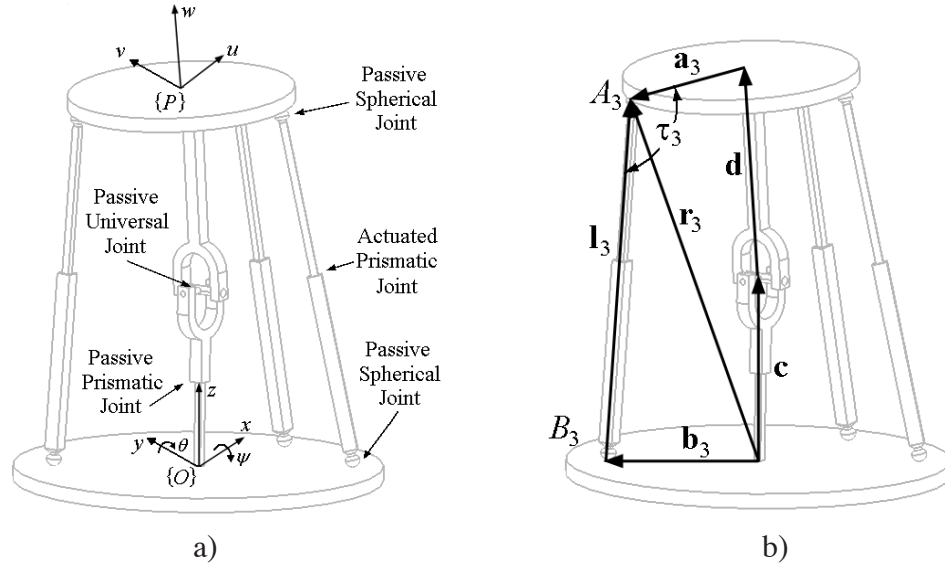


Figure 1: Tricept mechanism: a) basic structure and frames of reference and b) vector model for limb 3

When the moving platform is parallel to the base platform, the two revolute axes of the universal joint are parallel with the base frame's x and y axes. Because the orientation of the universal joint's second revolute axis (θ_2) is dependent on the rotation around the first (θ_1), a post-multiplication of individual rotation matrices must be performed:

$${}^O\mathbf{R}_P^* = \mathbf{R}_x(\theta_1) \mathbf{R}_y(\theta_2) \quad (10)$$

The two resulting matrices presented in equations (9) and (10) are numerically equivalent. It can easily be shown that the parasitic rotation around the z -axis can be obtained as:

$$s_\phi = \frac{s_{\theta_1} s_{\theta_2}}{c_\psi} \quad (11)$$

where θ_1 and θ_2 are determined by equating known terms of the rotation matrices ${}^O\mathbf{R}_P$ and ${}^O\mathbf{R}_P^*$.

Having solved for angles θ_1 and θ_2 , vector \mathbf{P} can be expressed in the base frame as:

$$\mathbf{p} = \mathbf{c} + {}^O\mathbf{R}_P^* \mathbf{P} \mathbf{d} = [ds_{\theta_2} \quad -ds_{\theta_1} c_{\theta_2} \quad c + dc_{\theta_1} c_{\theta_2}]^T \quad (12)$$

The only unknown in equation (12) is the displacement of the passive prismatic joint, c . Conveniently, this appears only in the solution for P_z which is defined and therefore c is easily determined. The remainder of the solution of the inverse displacement problem *i.e.*, solving for the actuated prismatic joint variables l_i , is a trivial exercise in vector algebra. Let r_p denote the magnitude of the end effector radius. Let α and β denote the angles made by vector \mathbf{a}_1 with vectors \mathbf{a}_2 and \mathbf{a}_3 respectively. These angles are defined as $\alpha = 120^\circ$ and $\beta = -120^\circ$. The position of the centre of the spherical joint of limb i , attached to

the moving platform expressed in terms of the moving frame $\{P\}$, *i.e.*, ${}^P\mathbf{a}_i$, may then be obtained by :

$${}^P\mathbf{a}_1 = [r_p \ 0 \ 0]^T, {}^P\mathbf{a}_2 = [r_p c_\alpha \ r_p s_\alpha \ 0]^T, {}^P\mathbf{a}_3 = [r_p c_\beta \ r_p s_\beta \ 0]^T \quad (13)$$

where c_α and s_α represent the cosine and sine of angle α , *etc.* These vectors, with respect to the base frame, are denoted by vector \mathbf{r}_i and may be expressed as:

$$\mathbf{r}_i = \mathbf{p} + {}^O\mathbf{R}_P^* {}^P\mathbf{a}_i \quad (14)$$

Letting r_b denote the base platform radius, the positions of the spherical joints connected to the base platform, with respect to the base frame $\{O\}$ are:

$$\mathbf{b}_1 = [r_b \ 0 \ 0]^T, \mathbf{b}_2 = [r_b c_\alpha \ r_b s_\alpha \ 0]^T, \mathbf{b}_3 = [r_b c_\beta \ r_b s_\beta \ 0]^T \quad (15)$$

Finally, the magnitude of each of the prismatic joints giving the final solution to the inverse displacement problem, may be expressed as follows for limb i :

$$l_i = |\mathbf{r}_i - \mathbf{b}_i| \quad (16)$$

2.2 Alternate Inverse Kinematics

The previously presented kinematics will serve as a tool to verify a more novel method of formulating the inverse kinematics for the given manipulator as follows, which will then in turn, be used to formulate the constraining Jacobian (\mathbf{P}). First, recall that the point A_i corresponds to the centre of the spherical joint connecting limb i to the moving platform. As suggested earlier in Section 1.1, the manipulator pose may be uniquely defined using the three z values, A_{i_z} (for $i = 1, 2, 3$). In this section, these three variables are deemed independent and will be used to define the remaining dependent end effector variables, namely A_{i_x} and A_{i_y} , the x and y -components of A_i (depicted in Figure 1b).

Generally, the choice of which of the potential 9 motions (A_{i_x} , A_{i_y} and A_{i_z}) to define as independent is not trivial. In this case, as the end effector translation along the z -axis is one of the defined independent degrees of freedom in section 2.1, at least one of the three A_{i_z} must be used here as an independent motion in the formulation of the alternate inverse kinematics. Choosing each of the three A_{i_z} values provides a consistent means of measuring and comparing the ability of each of the three limbs to alter the manipulator pose.

Consider again the vector sum equivalent to \mathbf{r}_i , written with respect to the base frame:

$$\mathbf{r}_i = \mathbf{c} + {}^O\mathbf{R}_P ({}^P\mathbf{d} + {}^P\mathbf{a}_i) \quad (17)$$

This vector \mathbf{r}_i describes point A_i with respect to the base frame. Therefore, the three A_{i_z}

coordinates may be written as:

$$A_{1z} = c + dc_{\theta_1}c_{\theta_2} - r_p(c_{\theta_1}s_{\theta_2}) \quad (18)$$

$$A_{2z} = c + dc_{\theta_1}c_{\theta_2} + r_p(-c_{\theta_1}s_{\theta_2}c_\alpha + s_{\theta_1}s_\alpha) \quad (19)$$

$$A_{3z} = c + dc_{\theta_1}c_{\theta_2} + r_p(-c_{\theta_1}s_{\theta_2}c_\beta + s_{\theta_1}s_\beta) \quad (20)$$

Independently subtracting equation (18) from (19) and (20) and rearranging results in the following two relations:

$$\frac{(A_{2z} - A_{1z})}{r_p(1 - c_\alpha)} = c_{\theta_1}s_{\theta_2} + \frac{s_{\theta_1}s_\alpha}{(1 - c_\alpha)} \quad (21)$$

$$\frac{(A_{3z} - A_{1z})}{r_p(1 - c_\beta)} = c_{\theta_1}s_{\theta_2} + \frac{s_{\theta_1}s_\beta}{(1 - c_\beta)} \quad (22)$$

Now, subtracting equation (22) from (21), and isolating s_{θ_1} :

$$s_{\theta_1} = \frac{\left[\frac{(A_{2z} - A_{1z})}{r_p(1 - c_\alpha)} - \frac{(A_{3z} - A_{1z})}{r_p(1 - c_\beta)} \right]}{\frac{s_\alpha}{(1 - c_\alpha)} - \frac{s_\beta}{(1 - c_\beta)}} \quad (23)$$

If the values A_{iz} are given, the only remaining unknown in equation (23) is s_{θ_1} . Obviously, two solutions exist for θ_1 . The range for θ_1 may be limited to $-90^\circ \leq \theta_1 \leq 90^\circ$ which is consistent with its intended application (machining). This provides a means to obtain a single solution for θ_1 within that range. Substituting this solution back into equation (22) and isolating s_{θ_2} :

$$s_{\theta_2} = \frac{\left[\frac{(A_{3z} - A_{1z})}{r_p} - s_{\theta_1}s_\beta \right]}{c_{\theta_1}(1 - c_\beta)} \quad (24)$$

Again, two possible solutions result but by limiting the range to within $-90^\circ \leq \theta_2 \leq 90^\circ$, a single solution is found. With these two angles, the remainder of the solution is identical to that of the conventional inverse displacement problem, commencing from equation (11). The first derivative of these equations, with respect to time will be used in the formulation of the Jacobian matrix, which is discussed in the following section.

2.3 Jacobian Formulation

In order to obtain the constrained, dimensionally homogeneous Jacobian matrix shown in equation (8), the Jacobian matrix in equation (3) must first be developed according to the methodology introduced by Kim and Ryu [8]. Consider a point anywhere on the plane defined by the three spherical joints connected to the moving platform. Let vector \mathbf{g} represent this point with respect to the base frame. This vector may be represented as an appropriately weighted sum of the three vectors \mathbf{r}_i :

$$\mathbf{g} = k_{i,1}\mathbf{r}_1 + k_{i,2}\mathbf{r}_2 + k_{i,3}\mathbf{r}_3 \quad (25)$$

where $k_{i,j}$ ($j = 1, 2, 3$) are dimensionless constants in the range (0,1). The values of these dimensionless constants may be easily solved using the system of three scalar equations in (25). Making the substitution $\mathbf{g} = \mathbf{r}_i = \mathbf{b}_i + \mathbf{l}_i$ into equation (25):

$$\mathbf{b}_i + \mathbf{l}_i = k_{i,1}\mathbf{r}_1 + k_{i,2}\mathbf{r}_2 + k_{i,3}\mathbf{r}_3 \quad (26)$$

where vector \mathbf{l}_i represents the actuated prismatic joint as in Figure 1b. Taking the first time derivative of equation (26):

$$\omega \times l_i \mathbf{s}_{l_i} + \dot{l}_i \mathbf{s}_{l_i} = k_{i,1} \dot{\mathbf{r}}_1 + k_{i,2} \dot{\mathbf{r}}_2 + k_{i,3} \dot{\mathbf{r}}_3 \quad (27)$$

where ω and \mathbf{s}_{l_i} are the angular velocity and unit vector associated with \mathbf{l}_i respectively. In order to eliminate ω from equation (27), the equation may be dot multiplied by \mathbf{s}_{l_i} :

$$\dot{l}_i = k_{i,1} \mathbf{s}_{l_i}^T \dot{\mathbf{r}}_1 + k_{i,2} \mathbf{s}_{l_i}^T \dot{\mathbf{r}}_2 + k_{i,3} \mathbf{s}_{l_i}^T \dot{\mathbf{r}}_3 \quad (28)$$

Writing this equation three times corresponding to each of three limbs produces the conventional inverse \mathbf{J}_q (where in this case $\mathbf{J}_q = \mathbf{I}_{3 \times 3}$) and direct \mathbf{J}_x Jacobian matrices:

$$\mathbf{J}_q \dot{\mathbf{q}} = \mathbf{J}_x \dot{\mathbf{x}} \quad (29)$$

where the multiplication $\mathbf{J}_q^{-1} \mathbf{J}_x$ produces the matrix \mathbf{J} in equation (3), $\dot{\mathbf{q}}$ is equivalent to that in equation (2). Recalling that when the point A_i is expressed in the base frame, it is equivalent to the vector \mathbf{r}_i , and the vector $\dot{\mathbf{x}}$ in equation (29) is equivalent to the one defined in equation (4).

Using the alternative form of the inverse kinematics presented in section 2.2, equations may be developed for each of the defined dependent motions A_{i_x} and A_{i_y} as functions of the defined independent motions A_{i_z} . The constraining matrix \mathbf{P} in equation (6) is produced by taking the first derivative with respect to time of these various equations, producing the various partial derivative entries. These equations include (17-24) which relate A_{i_z} to the universal joint angles θ_1 and θ_2 , and equations (11-16) relating θ_1 and θ_2 to the actuator displacements l_i . Finally, the matrix multiplication $\mathbf{J}\mathbf{P}$ results in the constrained, dimensionally homogeneous Jacobian in equation (8). Further details on the development of the constraining matrix may be obtained in [9]

3 WORKSPACE ANALYSIS

In this paper, the reachable workspace will be restricted to achievable poses without having passed through a singular configuration. Intuitively, there are two different families of singular configurations. The first is whenever any of the SPS limbs is parallel to the plane defined by the three spherical joints around the end effector platform or the equivalent plane in the base platform. The second family of singular configurations is defined by the central passive limb. Whenever vectors \mathbf{c} and \mathbf{d} are perpendicular, the passive limb has lost the ability for either rotating around the base frame's x or y axes. The computer algorithm determining the workspace size as a sum of areas in rad^2 contains both singular configurations as potential workspace boundary conditions.

A modified computer algorithm of that employed in [11] has been developed, correspond-

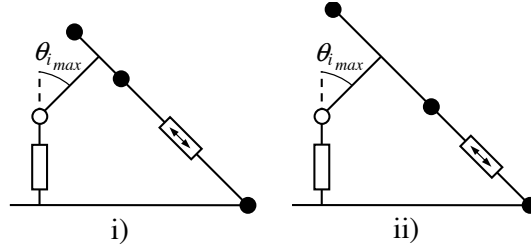


Figure 2: The direct singular configuration is obtained at the same pose regardless of the magnitude of r_p .

ing to the kinematics of the Tricept mechanism. The algorithm works by first discretizing the workspace into a user-specified number of z -slices and η -meridians. At each z -slice, the algorithm probes the boundaries of the workspace in η different directions.

3.1 Reachable Workspace

Poses resulting in a real and positive solution to the inverse displacement problem in equation (16), and obtained without passing through either of the singular configurations discussed above, are included in the reachable workspace. In addition, since the Tricept's workspace theoretically extends to infinity in the z -direction, a realistic limit on the stroke of the prismatic actuators must be imposed in order to obtain meaningful results. This paper will limit the highest attainable elevation to $z_{end} = 1$.

Angles α and β are omitted from this optimization study as it has already been shown in [11] that the optimal configuration for a similar mechanism is symmetric, *i.e.*, $\alpha = 120^\circ$ and $\beta = -120^\circ$. Remaining architectural variables are the end effector radius r_p , the base platform radius r_b , and the magnitude of vector, d . As Figure 2 shows, the magnitude of r_p has no influence on the size of the reachable workspace. In these depictions, solid circles represent spherical joints, the empty circle is the universal joint, empty rectangles are the passive prismatic joints, and actuated prismatic joints are represented by rectangles with arrows inside them aligned with the respective line of action of the joints. The direct singular configuration where one or more of the actuated limbs are parallel with the plane defined by the three spherical joints on the end effector platform, is obtained at the same pose, regardless of the magnitude of r_p . Therefore, it will be set to $r_p = 1$ and will be omitted from this optimization study.

The monotonical influence (within the considered ranges) of the last two remaining variables r_b and d on the reachable workspace size is depicted in Figure 3. In the first plot, $\frac{\partial^2 S}{\partial d^2}$ (the second derivative of size with respect to change in d) is not constant nor monotonic, as evidenced by the inflection point at $d \approx 0.8$. If $d = r_b$, some points on the reachable workspace boundary correspond to poses where both the direct singular configuration and the passive limb's singular configuration may exist simultaneously. At $d \ll r_b$, the manipulator does not reach the passive limb's singular configuration prior to the direct singular configuration, when moving from the datum position. However, at $d \approx 0.8$, the manipulator does begin to reach poses *near* the passive limb's singular configuration (*i.e.*, either θ_1 or $\theta_2 = 90^\circ$). In order to avoid these singular configurations, maximum values for θ_1 and θ_2 have been set to approximately 88.5° in the algorithm determining the workspace size.

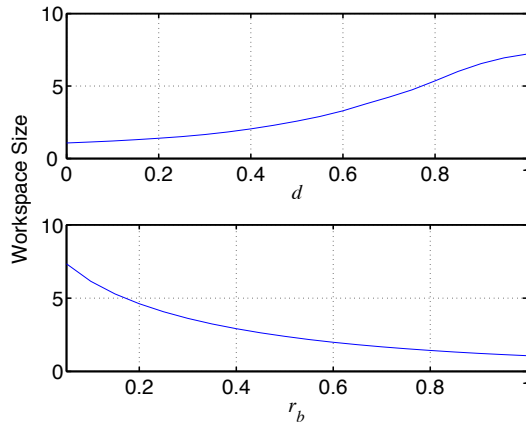


Figure 3: Reachable workspace size as functions of d and r_b . Default values are $d = 0$, and $r_b = 1$.

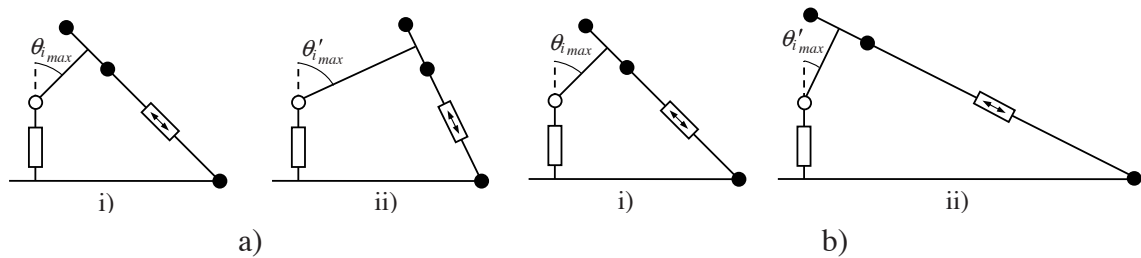


Figure 4: The direct singular configuration is obtained at a) a larger rotation of the universal joint with increasing magnitude of d and b) smaller rotation of the universal joint with increasing magnitude of r_b .

As indicated by the inflection point in Figure 3, the algorithm encounters this limit for θ_1 and θ_2 at $d \approx 0.8$,

Physical reasoning for the results in these plots are depicted in Figures 4a and 4b. As shown in 4a, the singular configuration is reached at a pose where the rotation around the universal joint (θ_{1max}) is larger if the magnitude of d is also larger. The opposite effect, *i.e.*, the reachable workspace size decreases, is realized by increasing the magnitude of the base radius, r_b (Figure 4b).

3.2 Dexterous Workspace

Mathematical definitions of dexterity have been discussed in [9]. In this work, both the condition number and a maximum allowable singular value of the constrained Jacobian matrix (**JP**) are used to define the dexterous workspace. These conditions guarantee that the manipulator maintains similar motion ability in each of its degrees of freedom **and** these motions are performed above a minimum acceptable velocity. In this way, the dexterous workspace is limited to poses where the manipulator maintains a minimum yet similar level of agility in each of its degrees of freedom.

Figure 5a depicts the dexterous workspace when defined by an arbitrarily chosen maximum

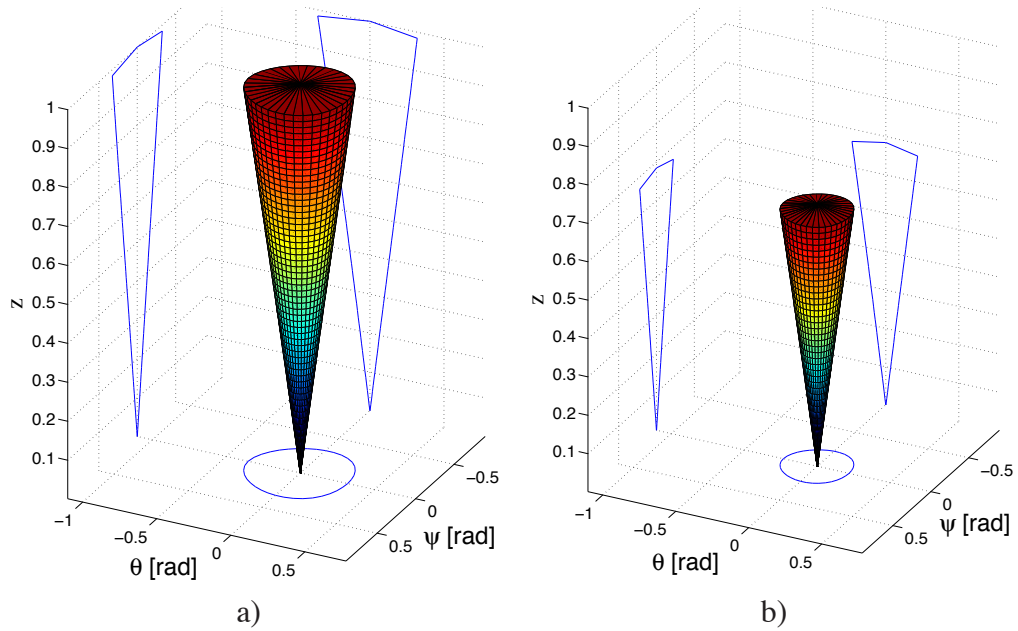


Figure 5: Dexterous workspace defined by a) a maximum condition number of 12 and b) both a maximum condition number of 12 and maximum singular value of 0.6. Architectural parameters are $r_p = r_b = 1$ and $d = 0$.

condition number of 12. That is, only poses where moving in one direction requires a minimum of $1/12$ of the effort required to move in another direction are included. Singular values σ in Figure 5a vary within the range $9.4087 \times 10^{-6} \leq \sigma \leq 0.73796$.

In Figure 5b, both a maximum condition number of 12 and maximum singular value, σ , of 0.6 are arbitrarily chosen to define the dexterous workspace. The result of Figure 5b has a very simple explanation. First, let the angle between vectors \mathbf{a}_i and \mathbf{l}_i be denoted by τ_i , as in Figure 1b. Higher end effector velocities may be obtained when the actuated limb has a high amount of leverage over the end effector platform, *i.e.*, τ_i is near 180° . This corresponds to lower elevations of the end effector platform, as depicted in Figure 5b.

Angles τ_i are very sensitive to the actuator displacement, and are an important feature in understanding the results of Figure 6. For instance, Figures 3 and 4a demonstrate the benefit of increasing the magnitude of d on the reachable workspace size. However, for poses where θ_1 , or $\theta_2 \neq 0$, this advantage is offset by the fact that as $|d|$ is increased, the maximum difference between the angles τ_i in the three limbs, *i.e.* $\Delta\tau = \tau_{\max} - \tau_{\min}$, also increases. The difference in leverage each actuated limb has over the end effector platform is analogous to the Jacobian matrix condition number. Therefore, although increasing $|d|$ nominally increases the reachable workspace size, it does not necessarily increase the subset, the dexterous workspace size.

Similarly, increasing the magnitude of r_p decreases angle τ in each limb, unless at the workspace boundary as depicted in Figure 2. This corresponds to an increase in the singular values of the Jacobian matrix. In addition, the difference in leverage, expressed by $\Delta\tau$, also increases. However, reducing r_p may not always be beneficial as shown in Figure 6. Although the leverage is increased as τ increases towards 180° , the pose of the manipulator

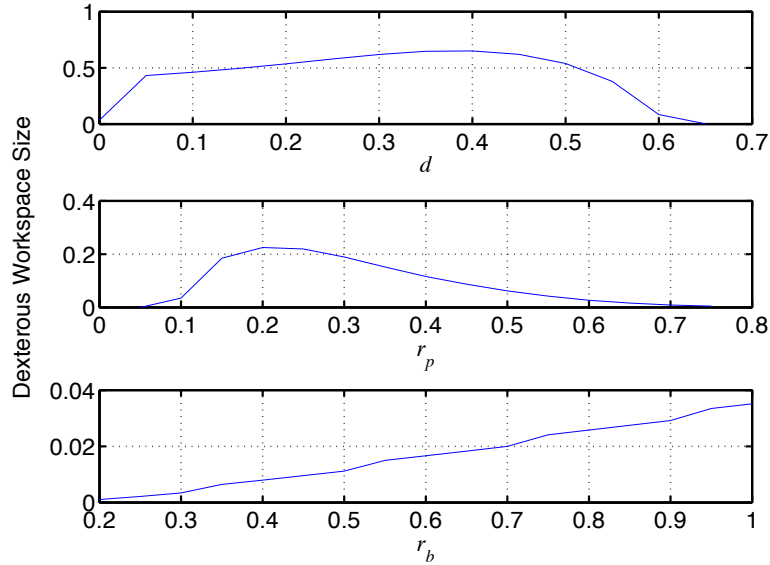


Figure 6: The dexterous workspace size as functions of d , r_p , and r_b . Default values are $d = 0$, $r_p = 0.1$, and $r_b = 1$.

appears closer to the direct singular configuration discussed earlier. This may explain the apparent optimum value of $r_p \simeq 0.2$ in this example.

Finally, as the magnitude of the base platform radius, r_b is increased, the angle τ is also increased for any pose. This corresponds to an ability to obtain higher end effector velocities for given actuator velocities. As r_b is increased $\Delta\tau$ decreases, resulting in a lower condition number. Although increasing the magnitude of r_b decreases the reachable workspace size, it increases the dexterous workspace size. It is logical to assume that at some point, the rate of loss in reachable workspace size will in turn correspond to a loss in dexterous workspace size, if the range of r_b in Figure 6 had been increased.

4 CONCLUSIONS

The inverse displacement solution for the Tricept mechanism where the independent degrees of freedom are defined as a translation along the z -axis and rotations around the x and y -axes has been provided. An alternate solution to the inverse displacement problem (also provided) shows that the manipulator pose may also be uniquely defined using the z -coordinates of three different points on the end effector platform.

A 3×9 Jacobian matrix is formulated based on the method introduced in [8]. A 9×3 constraining matrix may then be used to reduce the Jacobian to a square 3×3 . The entries of the constraining matrix are formulated using partial derivatives of the alternative inverse displacement solution. The resulting constrained Jacobian matrix relates the z -coordinate velocities of the three end effector points to the actuator velocities. The condition number and singular values of this matrix may further be used to define the dexterous workspace. The architectural variables of r_b (base platform radius) and d (offset within the passive leg) are identified as having an influence on the reachable workspace size. The third architectural variable, r_p (moving platform radius), is shown to have no influence. Within the

ranges tested, reachable workspace size is largest when small values of r_b and large values of d are used. The dexterous workspace is defined by manipulator poses where high end effector velocities may be obtained given a set of actuator velocities and furthermore, that this ability is common in each of the degrees of freedom. This is defined mathematically as poses where the condition number of the 3×3 constrained Jacobian matrix is below a specified limit, and where all singular values of the square, constrained Jacobian matrix (JP) must be below a specified threshold. All three architectural variables are found to have an influence on the dexterous workspace size. Their exact influence has been demonstrated. The influence of each variable was studied on an independent basis. Multivariable optimization may produce a different set of optimum architectural parameters.

BIBLIOGRAPHY

- [1] Neumann, K-E, US patent 4,732,525, Mar. 22, 1988, and affiliated reply to author.
- [2] Siciliano, B., Tricept robot: inverse kinematics, manipulability analysis and closed-loop direct kinematics algorithm, *Robotica*, **17**(4):437-445, 1999.
- [3] Zhang, D., and Gosselin, C. M., Kinetostatic analysis and design optimization of the Tricept machine tool family, *J. of Manuf. Science and Eng.*, **124**(3):725-733, 2002.
- [4] Joshi, S., and Tsai, L.-W, The kinematics of a class of 3-DOF, 4-legged parallel manipulators, *Journal of Mechanical Design*, **125**(1):52-60, 2003.
- [5] Joshi, S., and Tsai, L.-W, A comparison study of two 3-DOF parallel manipulators: One with three and the other with four supporting legs, *IEEE Transactions on Robotics and Automation*, **19**(2):200-209, 2003.
- [6] Xi, F., Zhang, D., Xu, Z., and Mechefske, C. M., A comparative study on tripod units for machine tools, *Int. J. of Machine Tools and Manufacture*, **43**(7):721-730, 2003.
- [7] Gosselin, C. M., The optimum design of robotic manipulators using dexterity indices, *Journal of Robotics and Autonomous Systems*, **9**(4):213-226, 1992.
- [8] Kim, S.-G., and Ryu, J., New dimensionally homogeneous Jacobian matrix formulation by three end-effector points for optimal design of parallel manipulators, *IEEE Transactions on Robotics and Automation*, **19**(4):731-737, 2003.
- [9] Pond, G. T., and Carretero, J. A., Formulating Jacobian matrices for the dexterity analysis of parallel manipulators, Submitted to *Mech. and Machine Theory*, Feb. 2005.
- [10] Carretero, J. A., Podhorodeski, R. P., Nahon, M. A., and Gosselin, C. M., Kinematic analysis and optimization of a new three degree-of-freedom spatial parallel manipulator, *Journal of Mechanical Design*, **122**(1):17-24, 2000.
- [11] Carretero, J. A., Nahon, M. A., and Podhorodeski, R. P., Workspace analysis and optimization of a novel 3-DOF parallel manipulator, *International Journal of Robotics and Automation*, **15**(4):178-188, 2000.